Itinerant G-type antiferromagnetism in $D0_3$-type V_3Z (Z = Al, Ga, In) compounds: A first-principles study

Iosif Galanakis,[1,*] Şaban Tırpancı,[2] Kemal Özdoğan,[3] and Ersoy Şaşıoğlu[4,†]
[1]*Department of Materials Science, School of Natural Sciences, University of Patras, GR-26504 Patra, Greece*
[2]*Department of Physics, Gebze Technical University, 41400 Gebze, Kocaeli, Turkey*
[3]*Department of Physics, Yildiz Technical University, 34210 İstanbul, Turkey*
[4]*Peter Grünberg Institut and Institute for Advanced Simulation, Forschungszentrum Jülich and JARA, D-52425 Jülich, Germany*
(Received 18 April 2016; revised manuscript received 26 May 2016; published 1 August 2016)

Heusler compounds are widely studied due to their variety of magnetic properties making them ideal candidates for spintronic and magnetoelectronic applications. V_3Al in its metastable $D0_3$-type Heusler structure is a prototype for a rare antiferromagnetic gapless behavior. We provide an extensive study on the electronic and magnetic properties of V_3Al, V_3Ga, and V_3In compounds based on electronic structure calculations. We show that the ground state for all three is a G-type itinerant antiferromagnetic gapless semiconductor. The large antiferromagnetic exchange interactions lead to very high Néel temperatures, which are predicted to be around 1000 K. The coexistence of the gapless and antiferromagnetic behaviors in these compounds can be explained considering the simultaneous presence of three V atoms at the unit cell using arguments which have been employed for usual inverse Heusler compounds. We expect our study on these compounds to enhance further the interest on them towards the optimization of their growth conditions and their eventual incorporation in devices.

DOI: 10.1103/PhysRevB.94.064401

I. INTRODUCTION

The constant growth of computational materials science triggered an even more exciting growth in experimental materials science. Several phenomena have been explained based on *ab initio* electronic structure calculations and several compounds with predefined properties targeting at specific applications have been studied. Among them exist the so-called half-metallic Heusler [1] compounds a special class of magnets which present semiconducting behavior for one of the two spin channels [2,3]. Several Heusler compounds have been identified using *ab initio* calculations prior to their experimental growth [4,5]. Such materials can find a variety of applications in the field of magnetoelectronics (nanoelectronics where only magnetic materials are employed) and spintronics (nanoelectronics where hybrid devices of semiconductors and magnetic materials are used) [6]. We should note here that there are also other known half-metals like $La_{0.7}Sr_{0.3}MnO_3$ which have been also demonstrated to present fully spin-polarized tunnelling in magnetic tunnel junctions [7], but Heusler compounds remain very attractive for applications due to their very high Curie temperatures and their structural similarity to binary semiconductors [8,9].

The most studied Heusler compounds in literature are the so-called full Heuslers having the chemical formula X_2YZ, like Co_2MnSi, and several have been identified as half-metals [10]. When the valence of the X is smaller than the valence of the Y they are called inverse Heusler compounds and crystallize in a similar structure where only the sequence of the atoms changes [11]. Also most of the latter compounds are half-metallic magnets [11]. Although the compounds referred to above can find several applications in spintronics and magnetoelectronics [12], several half-metallic Heusler compounds with more exotic properties have been found which can further optimize the operation of devices. Among them are the so-called spin-gapless semiconducting (SGS) [13] Heuslers which present a usual semiconducting band structure for one spin direction and a gapless (almost or exactly zero energy gap) in the other spin direction [14,15]. Such materials can enhance the performance of devices since vanishing energy is needed to excite both electrons and holes and a prototype Mn_2CoAl has been already grown experimentally and its SGS properties have been confirmed [16].

A material of special interest is V_3Al, a Heusler compound crystallizing in the so-called $D0_3$ lattice structure shown in Fig. 1, which resembles the cubic structure of full Heuslers where now all X an Y atoms are identical, adopted also by other materials like Fe_3Al, Fe_3Si, and Cr_3Se [17,18]. The first attempt to study this material using first-principles calculations predicted a nonmagnetic ground state [19]. But latter calculations by Skaftouros and collaborators predicted that the ground state is in reality an antiferromagnetic gapless semiconductor [14] resembling the well-known gapless semiconductors [20]. Such an electronic structure is possible since as shown in Fig. 1 there are two V atoms sitting at the A and C sites which form a simple cubic structure, if we neglect the other sites. The V atoms at these sites are allowed due to symmetry to have antiparallel spin magnetic moments of the same size leading to G-type antiferromagnetism shown schematically also in Fig. 1. The V atoms at the B sites and the Al atoms at the D sites are at the center of a cube surrounded by four V atoms at A sites and four V atoms at C sites and thus due to symmetry reasons their spin magnetic moment in such a configuration should be zero. This is compatible with the so-called Slater-Pauling rule connecting the total number of valence electrons to the total spin magnetic moment in Heusler compounds [11]. In 2015 Jamer and collaborators presented an extensive study on V_3Al combining both electronic structure calculations and experiments [21]. On one hand, their simulations confirmed

*galanakis@upatras.gr
†e.sasioglu@gmail.com

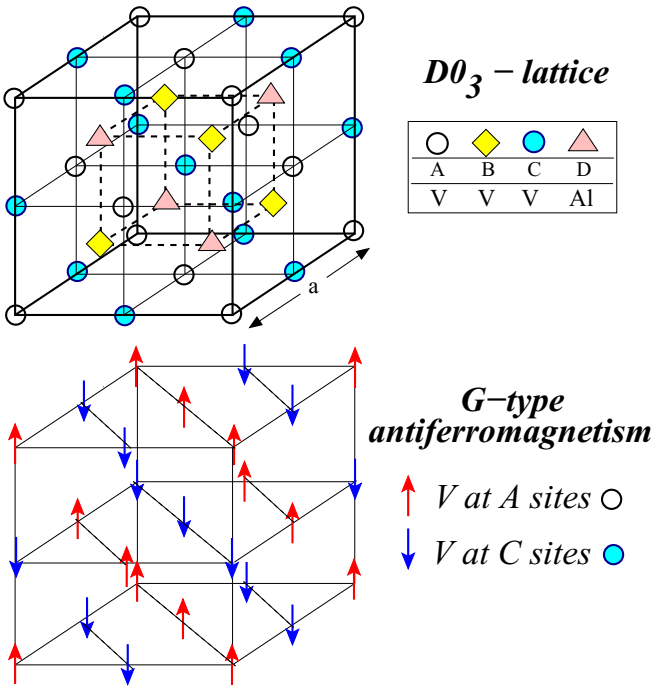

FIG. 1. Upper panel: schematic representation of the cubic $D0_3$ structure adopted by the V_3Z Heusler compounds. The unit cell is that of an fcc with four equidistant atoms as basis along the [111] diagonal. The atoms at the A and C sites are at the center of a cube surrounded by four atoms at the B and four atoms at the C sites and vice versa. The V next-nearest neighboring atoms at the A and C sites form a lattice of octahedral symmetry if we neglect the B and D sites. Lower panel: schematic representation of the *G*-type antiferromagnetic order made up of successive (111) planes which are antiferromagnetically coupled. The V atoms at the A and C sites have antiparallel spin magnetic moments denoted by arrows of opposite direction. The V atoms at the B sites and the Al atoms have zero spin magnetic moments due to symmetry reasons being situated at the center of cubes having four V atoms at the A sites and four V atoms at C sites as nearest neighbors.

the results of Skaftouros *et al.* and, on the other hand, they have successfully grown films of V_3Al and dichroic experiments using synchrotron radiation were compatible with an antiferromagnetic state. Here we have to note that the ground state of V_3Al is not the Heusler structure but the A15 lattice structure and V_3Al in this structure is a well-known superconductor [22,23].

V_3Al can be viewed as a prototype material for studying gapless antiferromagnetic behavior and can be considered as a cornerstone for future spintronic and magnetoelectronic devices based on antiferromagnetic elements. Thus in the present paper we provide an extensive study based on simulations of the electronic and magnetic properties of V_3Al as well as of the stability of its antiferromagnetic character. To make our study more complete we have also included results on V_3Ga and V_3In compounds which have the same number of valence electrons. Also these compounds were found to be antiferromagnetic gapless semiconductors and thus we will mainly concentrate on V_3Al but conclusions are also valid for them. We should note that for the Heusler compounds, the number of valence electrons plays the main role in determining their electronic and magnetic properties and thus it is expected that all three compounds under study present similar properties (see, e.g., Ref. [24]). In Sec. II we shortly present the computational method. In Sec. III A we discuss the electronic properties and the gapless behavior of the V_3Al compound under study and in Sec. III B its magnetic properties, including also the calculation of the exchange constants and the Néel temperature. Section III C is devoted to the origin of the gapless behavior. Finally in Sec. IV we summarize and present our conclusions. We believe that our present results will even further intensify the interest on this unique compound.

II. COMPUTATIONAL METHOD

To perform the electronic structure calculations, we employed the full-potential nonorthogonal local-orbital minimum-basis band structure scheme (FPLO) [25,26] within the generalized gradient approximation (GGA) as parametrized by Perdew, Burke, and Ernzerhof [27]. Some of the results presented in Secs. III A and III B have been also obtained using the local-spin-density approximation (LSDA) [28]. We have used the lattice parameter of 6.09 Å calculated via total energy calculations also using the FPLO method within GGA in Ref. [14]. Using the same method we have also calculated the equilibrium lattice constants for the other two compounds and found a value of 6.07 Å and 6.32 Å for V_3Ga and V_3In, respectively (see Table I). For the integrations in the first Brillouin zone a dense Monkhorst-Pack grid has been used [29]. All results presented in this study have been obtained using FPLO with the exception of the exchange constants and Néel temperature in Sec. III B, which are obtained employing the ASW method [30].

To calculate interatomic exchange parameters we employ the frozen-magnon technique [31–33] as described in Refs. [24–34]. The Néel temperature is estimated by employing the so-called random-phase-approximation (RPA) approach [34–38].

TABLE I. Calculated lattice parameters, total energy differences between nonmagnetic and antiferromagnetic states, and atom-resolved spin magnetic moments (in μ_B) employing the FPLO method for the $D0_3$-type V_3Z (Z = Al, Ga, In) compounds. In parentheses we show the spin magnetic moments obtained employing the ASW method which are also used to calculate the Néel temperatures in the last column using both the GGA and LSDA (temperature values in parenthesis) functionals.

Compound	a (Å)	ΔE (eV)	m_V^A (GGA)	m_V^A (LSDA)	m_V^B	m_V^C (GGA)	m_V^C (LSDA)	m_Z^D	T_N^{RPA} (K)
V_3Al	6.09	−0.12	−1.65 (−1.58)	−1.12 (−1.26)	0.00	1.65 (1.58)	1.12 (1.26)	0.00	988 (648)
V_3Ga	6.07	−0.10	−1.55 (−1.43)	−1.02 (−1.08)	0.00	1.55 (1.43)	1.02 (1.08)	0.00	858 (512)
V_3In	6.32	−0.18	−1.98 (−1.74)	−1.48 (−1.43)	0.00	1.98 (1.74)	1.48 (1.43)	0.00	1023 (704)

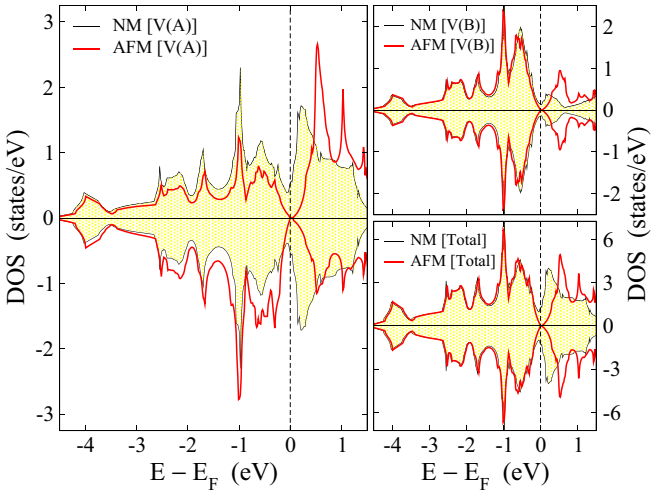

FIG. 2. Total and atom-resolved density of states (DOS) within GGA for the nonmagnetic (NM) and antiferromagnetic (AFM) magnetic configurations of V_3Al. Positive (negative) DOS values correspond to the spin-up (spin-down) electrons. The Fermi level corresponds to the zero energy.

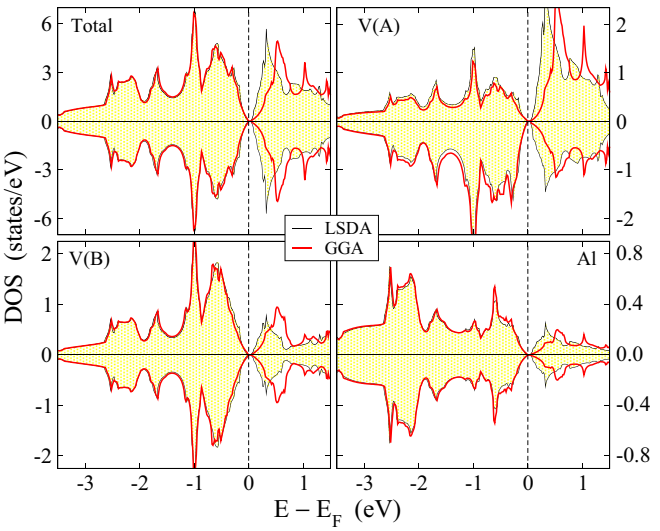

FIG. 3. GGA vs LSDA calculated DOS for the antiferromagnetic V_3Al compound. Details as in Fig. 2.

III. RESULTS AND DISCUSSION

A. Electronic properties and gapless behavior

First, we should establish the gapless behavior of V_3Al. To this end in Fig. 2 we have plotted the density of states (DOS) projected on the V atoms at the A and B sites (the site is written either in parenthesis or as superscript to distinguish the V atoms) as well as the total one in the unit cell for both the nonmagnetic (NM) and the antiferromagnetic (AFM) configurations. We should first note that we cannot use the terms majority and minority spin since there is an equal number of electrons of different spin in the formula unit; we will use the term spin-up for the positive DOS values and spin-down for the negative DOS values. We have also chosen the spin-up in the case of the V^A atoms such that its spin magnetic moment in Table I is negative. In the AFM case the DOS of the V^C atoms is identical to the V^A atoms exchanging the spin-up and spin-down electronic states. In the AFM case one gets a gapless behavior and the valence and conduction bands touch each other at the Fermi level. If we compare the NM and AFM calculations, most of the changes occur at the V^A DOS where the weight of the states around the Fermi level increases and we have a normal semiconductor. Deeper in energy the NM and AFM DOS are almost identical. Especially for the V^B atoms the DOS below the Fermi level is identical for both NM and AFM calculations. This also may explain the stability of the AFM case. A close examination of the total DOS reveals that the NM and AFM DOS are similar throughout most of the energy range but at the Fermi level the zero DOS at the AFM case leads to smaller values of the total energy stabilizing it against the NM case where more electronic charge is present at the Fermi level.

To establish the gapless semiconductor we have also performed calculations using the LSDA functional and present them in Fig. 3 versus the GGA results. LSDA is well known to underestimate the equilibrium lattice constants and to overestimate hybridization between orbitals with respect to GGA, but for the same lattice constant both LSDA and GGA should produce similar electronic properties. This is true since also LSDA reproduces the gapless semiconducting behavior of GGA. The only noticeable difference between the two functionals is the distribution of the weight of the unoccupied states just above the Fermi level. LSDA yields a smaller exchange splitting between *d* states of different spin at the V^A and V^C states and thus there is a small shift of the unoccupied states towards smaller energy values which also reflects on the DOS of the V^B and Al atoms.

B. *G*-type antiferromagnetism: Stability, magnetic moments, exchange constants and T_N

In this subsection we will discuss the magnetic properties of the compounds under study. In Table I we have included the energy difference ΔE between the nonmagnetic and the antiferromagnetic configurations. For all three compounds ΔE is negative meaning that the AFM state is the ground one reflecting the discussion in the last subsection of the previous section. The values vary between -0.10 and -0.18 eV, which are sizeable and suggest that the magnetic state should be feasible to stabilize in experiments like the ones of Jamer and collaborators [21]. Also in Table I we have included the atomic spin magnetic moments using the FPLO method within the GGA and LSDA approximations. The V^B and Al atoms have zero spin magnetic moments as expected since they are at the midpoints between the V^A and V^C atoms. The latter ones show considerable values of atomic spin magnetic moments, whose absolute values range within GGA from $1.55\mu_B$ in the case of V_3Ga to $1.98\mu_B$ for V_3In giving a first hint that exchange interactions should be strong leading to large values of the Néel temperature. In Table I we have also included the calculated spin magnetic moments employing the ASW method since the latter are used to calculate the exchange constants and the Néel temperatures. Both FPLO and ASW methods give similar electronic structure for the compounds under study and similar

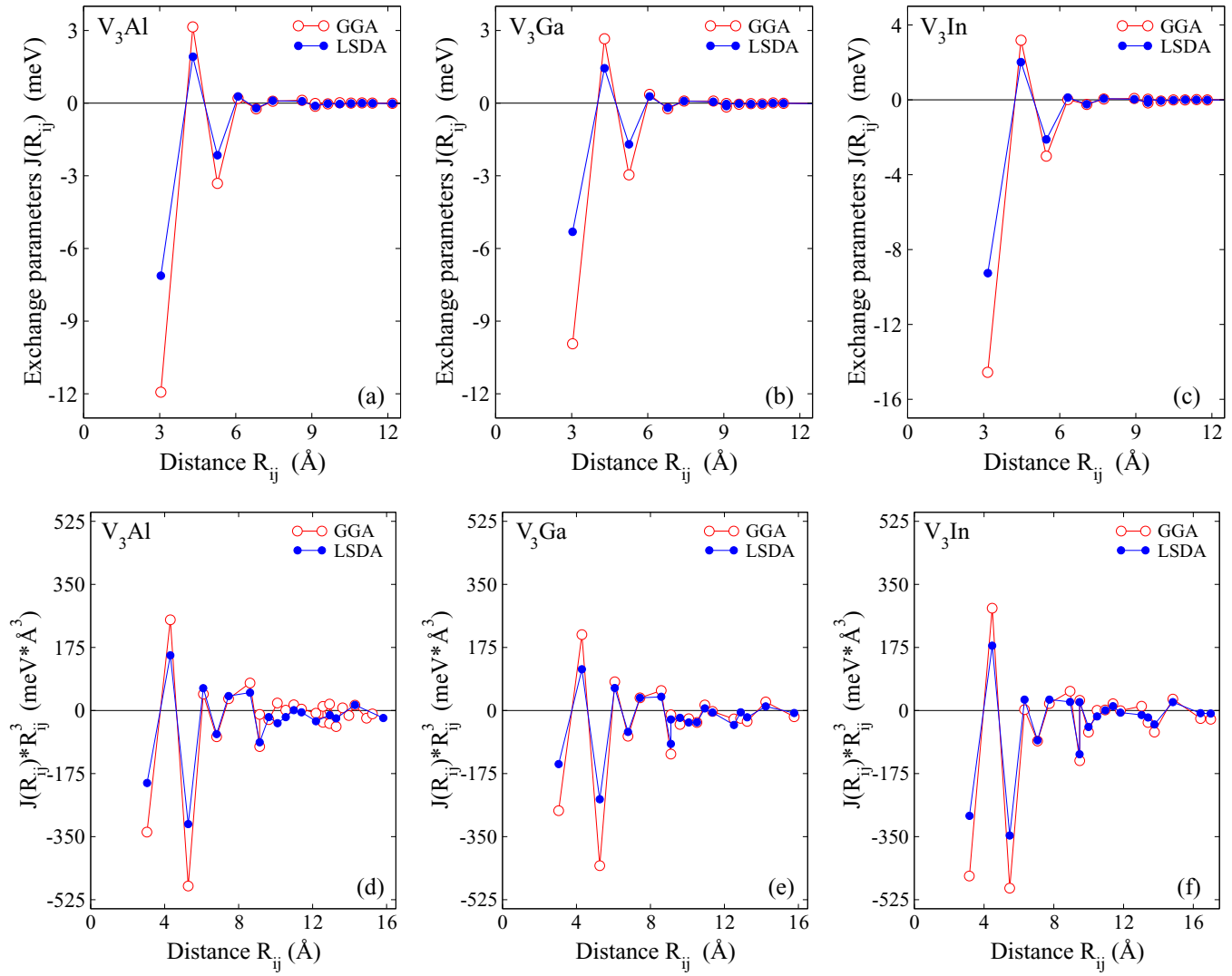

FIG. 4. Upper panel: interatomic exchange parameters (intersublattice V^A-V^C and intrasublattice V^A-V^A) as a function of the distance for all three compounds under study using both GGA and LSDA functionals. Lower panel: exchange parameters presented in the upper panel multiplied by the third power of the interatomic distance. This quantity also goes quickly to zero suggesting short-range and not RKKY-like interactions.

values of the spin magnetic moments. The only noticeable difference is that within FPLO the difference between the GGA and LSDA calculated spin magnetic moments is larger than within ASW. This should be attributed to the fact that FPLO is a full-potential method, while ASW is based on the atomic-spheres approximation (ASA) [39]. Finally, if one looks at the structure presented in Fig. 1 neglecting the V^B and Al atoms, one can consider the structure of being built up by successive (111) plane made up of either pure V^A or V^C atoms. Thus two successive (111) planes have atoms of antiparallel spin magnetic moments and antiferromagnetism is of the so-called *G* type shown in the lower panel of Fig. 1.

In the upper panel of Fig. 4 we present the calculated interatomic (intrasublattice and intersublattice) exchange parameters involving the magnetic V atoms as a function of the distance using the ASW results. We can easily deduce from the figure that only interactions within the first three coordination shells are sizable. The first coordination shell concerns the intersublattice V^A-V^C exchange interactions (each V^A atom has V^B and Al atoms, which have zero spin magnetic moment, as nearest neighbors and six V^C atoms as next nearest neighbors) and it is the largest one providing the dominating contribution to the formation of the antiferromagnetic ground state and to the Néel temperature. The second coordination shell refers to the intrasublattice V^A-V^A exchange interactions and it is of ferromagnetic character stabilizing further the antiferromagnetic state. Its value is considerably smaller than the absolute value of the exchange interaction between atoms in the first coordination shell due to the large distance between the V^A atoms in the lattice with respect to the V^A-V^C distance. As shown in the band structure presented in Fig. 8, the number of available states around the Fermi level, which affect the RKKY oscillations, is small. Thus the Drude term in the response function, which is responsible for the long-range interactions, is vanishing leading to a quick decay of the exchange constants (for an extended discussion, see Ref. [40]). To confirm our statement that the interactions are short range and not RKKY like, we have plotted in the lower part of Fig. 4

the product of the exchange constants and the third power of the interatomic distance. This quantity also vanishes quickly and thus the exchange constants decay faster than the inverse of the third power of the interatomic distance suggesting that no RKKY-like exchange mechanism is present [41]. This type of short-range behavior is typical of most half metallic magnets [34,41],

RPA estimated Néel temperatures, T_N^{RPA}, within GGA are presented Table I. V_3Al shows a T_N^{RPA} value of 988 K, V_3Ga of 858 K, and V_3In of 1023 K. All these values are much larger than the room temperature ensuring that devices based on these compounds would be functional at room temperature. The experiments by Jamer and collaborators have provided a value of about 600 K for V_3Al [21], which is considerably smaller than our value although it is still high compared to the room temperature. A possible source of this discrepancy could be that in Ref. [21] experiments were carried out on a film. For the spin-gapless semiconducting Mn_2CoAl compound, the experimental Curie temperature is 720 K for bulklike samples [16], while for thin films a value of 550 K is obtained [42]. *Ab initio* based estimations of the Curie temperature yield a value slightly larger than the bulk value of 720 K (see Ref. [15] and references therein).

Although the combination of GGA and RPA often provides a good estimation of the critical temperature values in Heusler compounds [34], it would be interesting to examine also the results of LSDA. As mentioned above LSDA overestimates the hybridization effect with respect to GGA resulting in considerably smaller values of the atomic spin magnetic moments in Table I. For example, the absolute values of the FPLO-computed V atomic spin magnetic moments in V_3Al decreases from $1.65\mu_B$ within GGA to $1.12\mu_B$ within LSDA a reduction of about 32%. The smaller atomic spin magnetic moments also affect the exchange interactions in Fig. 4, which are smaller within LSDA resulting in smaller predicted values of the T_N^{RPA} in Table I.

To discuss whether the magnetism is of localized or itinerant character, we study the behavior of the atomic spin magnetic moments under compression and present our results in Fig. 5 where we have plotted the GGA atomic spin magnetic moments under compression. As we compress the lattice and the lattice constant is reduced, the absolute values of the spin magnetic moments of both V^A and V^C atoms present a linear reduction vanishing at about 5.4 Å and the compound remains a perfect antiferromagnet under this compression. Thus the magnetic order vanishes for a value of ~10% compression of the lattice. Itinerant magnetic moments are reduced much faster than the localized ones since compression reduces the hybridization effects fast and eventually kills magnetism. Thus the question is whether such a threshold of 10% can characterize the magnetism in V_3Z compounds. In the case of Cr_3Se where both kinds of magnetic behaviors coexist [18], a 7% compression of the lattice constant completely kills spin magnetic moments of itinerant character, while the ones of localized character only slightly decrease [18]. In the case of the Ni_2MnSn Heusler compounds, which is a prototype of localized magnetism, an almost 30% compression of the lattice constant is needed to kill the local spin magnetic moments [43]. Moreover, as shown in Fig. 4 of Ref. [40], in the case of local magnetic moments

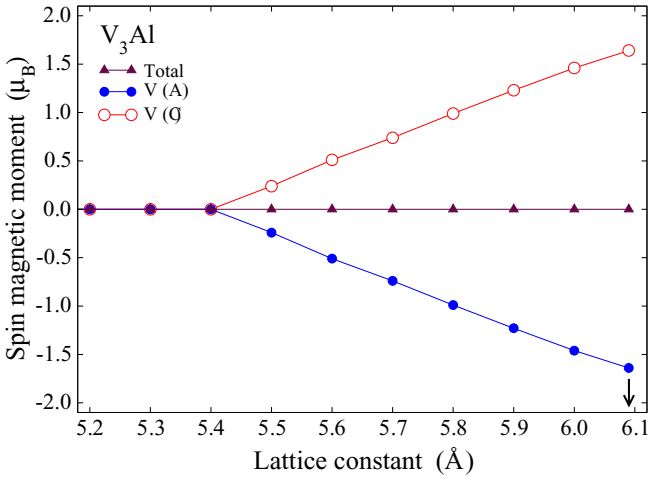

FIG. 5. Atomic and total spin magnetic moments in the case of V_3Al upon compression starting from the equilibrium lattice constant marked by an arrow. Note that spin magnetic moments of the V atom at B site and Al atom at D site are zero due to symmetry reasons.

their absolute values remain practically the same for both ferromagnetic and antiferromagnetic configurations, while in our case as we will discuss in the next paragraph the magnitude of the atomic spin moments vanishes at the ferromagnetic configuration. Thus the behavior of the magnetic spin moments in V_3Z compounds is compatible with an itinerant character of the magnetism.

Our final step in the investigation of the magnetic properties of the compounds under study is the stability of the AFM state with respect to ferromagnetic ordering. In Fig. 6 we have plotted for V_3Al the variation of the absolute values of the atomic spin magnetic moments of the V atoms at the A and C sites (left panel) as a function of the polar angle θ. On the right panel we plotted the behavior of the total energy

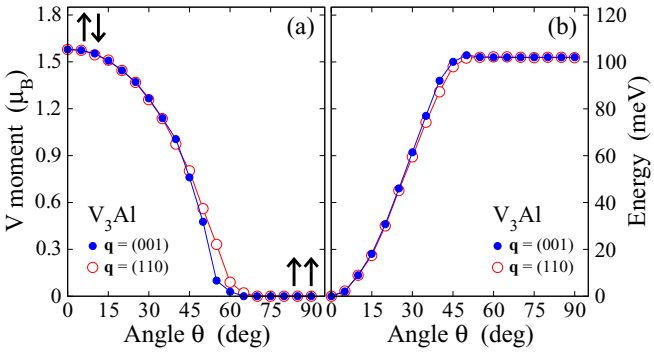

FIG. 6. Behavior of the absolute values of the atomic spin magnetic moments of the V atoms at the A and C sites (left panel) and of the total energy (right panel) as a function of the polar angle θ (see Ref. [40]) for two different values of the wave vector **q** (in units of $\frac{2\pi}{\alpha}$) in the case of the V_3Al compound. By varying θ between 0° and 90° for both wave vectors (001) and (110), the magnetic structure transforms continuously from the antiferromagnetic to the ferromagnetic configuration. We have also performed calculations for the (111) wave vector, but results are almost identical to the case of the (110) wave vector and thus we do not present them in the figure.

as a function of the polar angle. We took into account three different values of the wave vector **q** (in units of $\frac{2\pi}{\alpha}$): the (001), (110), and (111). For the latest case, the (111) wave vector, results are almost identical to the case of the (110) wave vector and thus we do not present them in Fig. 6. The reason for this choice is that for these values of wave vectors the magnetic structure transforms continuously from the antiferromagnetic to the ferromagnetic configuration as the θ angle changes from 0° to 90°. The curves for both **q** values presented in the figure are similar leading to the same conclusions. As the angle θ increases and the spin magnetic moments rotate to the ferromagnetic configuration the absolute values of the spin moments decrease and simultaneously the total energy increases reaching a maximum at about 45°. The minimum of the total energy corresponds to an angle of 0° and thus to the antiferromagnetic coupling of the spin magnetic moments of the V^A and V^C atoms.

C. Origin of the gapless behavior

In the last part of the discussion of the results, we will concentrate on the origin of the gapless behavior using arguments similar to the one used for the full and the inverse Heusler compounds [10,11]. Again we will use V_3Al as the prototype but results are similar also for the V_3Ga and V_3In compounds. As for the full Heuslers, we can have two type of *d* orbitals first the ones concentrated exclusively at the V^A and V^C sites. These atoms create a simple cubic structure, if we neglect the V^B and Al atoms, and thus due to symmetry reasons *d* hybrids of *u* type obeying the octahedral symmetry and being localized exclusively at the V^A and V^C sites are allowed. These can be distinguished between the double-degenerate e_u and the triple-degenerate t_{1u} states. Except the states of the *u* character we can also have states of *g* character which obey both the octahedral and tetrahedral symmetry and are delocalized to all sites. They also break down to the double-degenerate e_g and the triple-degenerate t_{2g} states. In the tetrahedral symmetry the e_g states are lower in energy than the t_{2g} states, while in the octahedral symmetry it is vice versa and the t_{1u} states are below the e_u states. In Fig. 7 we have projected the atom-resolved DOS on the different *g* and *u* states. Note that we cannot distinguish the $e_u(t_{1u})$ from the $e_g(t_{2g})$ states. The V^A and V^C atoms possess states of both character from both sides of the gap. In the case of V^B atoms, the states deeper in energy are of e_g character, while below the Fermi level states are exclusively of t_{2g} character (note that the *u* states are not allowed at the V^B site). Above the Fermi level we can find states of both characters.

To make a step further in our understanding of the origin of the gapless semiconducting behavior we have plotted in Fig. 8 the band structure along the K-Γ and Γ-X lines. Note that the band structure is identical for both spin directions. Examining the band structure along several directions (not shown here) reveals that there is a direct gap of vanishing width located at about the $\frac{1}{4}$ the K-Γ distance. Just below the Fermi level there is a triple-degenerate (at the Γ-point) band. Deeper in energy at about -2.5 eV below the Fermi level, at the Γ point there are very close in energy a triple and a double degenerate bands. Lower in energy (not shown here) is a single band. Above the Fermi level we have a triple-degenerate (at the Γ-point) band

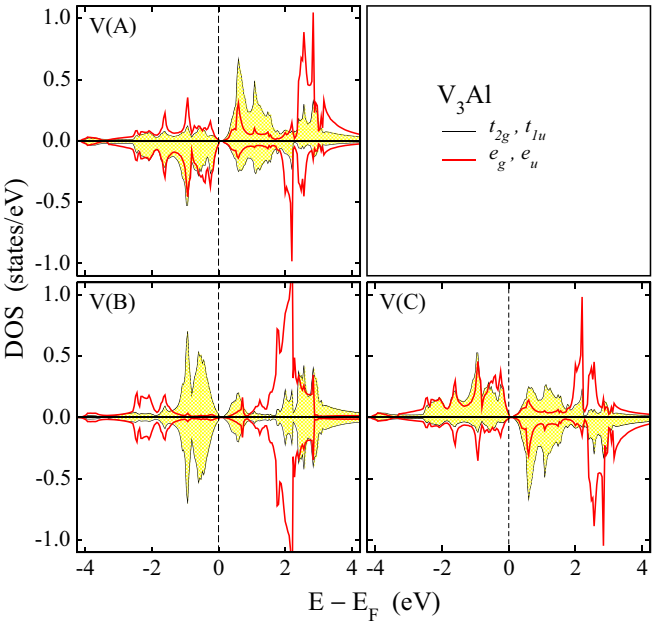

FIG. 7. DOS for the V atoms in V_3Al projected on the double degenerate e_g and e_u, and the triple degenerate t_{2g} and t_{1u} *d* states. Note that we cannot distinguish between the *g*-type states obeying both the octahedral and tetrahedral symmetry and the *u*-type states obeying exclusively the octahedral symmetry.

followed by two double-degenerate (at the Γ-point) bands. The character of the bands at the Γ point is primordial for our understanding of the origin of the gapless behavior since it reveals also the character of the bands at the real space and it has been extensively used in the case of Heusler compounds [10,11].

To reveal the character of each band we have performed an analysis based on the fat band scheme which we have also employed in the case of the Cr_3Se compounds in Ref. [18]. We do not show all band structure here but we resume our results in Fig. 9 where for one spin direction we present the

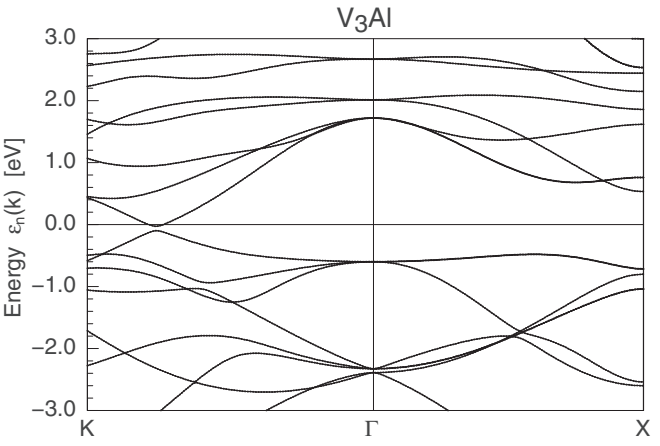

FIG. 8. Band structure along two high-symmetry axis. There is a direct gap at about one-fourth the distance between the K and the Γ high symmetry points. For the character of the bands see Fig. 9 and discussion in the text

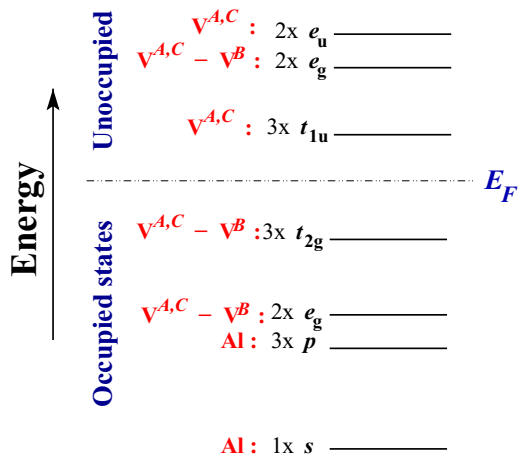

FIG. 9. Schematic representation of the character of the bands at the Γ point which corresponds to the character of the orbitals in real space, based on the atom and orbital resolved bands using the fat band scheme (not shown here). Notice that the low-lying Al p bands accommodate also a large portion of V's d charge and thus have a strong admixture of the $V^{A,C}$ triple-degenerate t_{2g} states.

character of the bands. First, we have to note that V_3Al has 18 valence electrons per formula unit (it coincides with the per unit cell value) and thus per spin we should have nine occupied states. As for the minority-band structures of full and inverse Heusler compounds which show the semiconducting behavior (see Refs. [10,11]), the single band low in energy stems from the Al valence s state. At about −2.5 eV there are very close in energy at the Γ point the triple-band stemming from the Al p states accommodating also d charge from the V atoms, and the double-band stemming from the e_g states which are spread over all V atoms. Just below the Fermi level the triple degenerate valence band has a t_{2g} character and the corresponding orbitals are located at all V sites; these bands have also a strong Al p admixture since the t_{2g} states when expressed around the Al site have a p character. The first bands above the Fermi level are the triple-degenerate t_{1u} bands located exclusively at the V^A and V^C sites followed by the e_g and e_u bands. Thus the Fermi level is located between the occupied t_{2g} and the empty t_{1u} states. This resembles the hybridization scheme in the case of the Sc- and Ti-based inverse Heusler compounds in Ref. [11]. The gap in the latter case is small since it does not result from a bonding-antibonding hybrid formation, and in the case of V_3Al its width is vanishing since both X and Y atoms in the X_2YZ formula of the inverse Heuslers are identical and the energy levels in the upper panel of Fig. 3 in Ref. [11] are much closer closing the gap separating the t_{2g} and the t_{1u} states. This describes the gapless character of V_3Al.

IV. CONCLUSIONS

Heusler compounds are widely studied due to their variety of magnetic properties and their potential applications in spintronics and magnetoelectronics. We have provided an extensive study on the electronic and magnetic properties of V_3Al Heusler compound as well as its isovalent V_3Ga and V_3In compounds using state-of-the-art electronic structure calculations. All compounds prefer the gapless G-type antiferromagnetic structure. The large absolute values of the spin magnetic moments of the V atoms having antiparallel spin moments lead to a strong short-range exchange interaction and consequently to large values of the Néel temperature which approaches or even exceeds 1000 K, making them operational at room temperature. The G-type antiferromagnetism is stable with respect to the ferromagnetic configuration and it proves to be of strongly itinerant character. Finally, we discussed the origin of the gapless behavior. We have shown that the character of the bands is similar to the inverse Heusler compounds studied in Ref. [11] but the presence of three V atoms at the unit cell closes the gap leading to the gapless character.

We expect our study on V_3Al, V_3Ga, and V_3In compounds to enhance further the interest on them. Based on our results and the experiments in Ref. [21], further experiments are needed to establish a grown mechanism optimizing the magnetic and structural properties of these compounds in the metastable Heusler structure leading to their eventual incorporation in devices.

[1] F. Heusler, Verh. Dtsch. Phys. Ges. **12**, 219 (1903).
[2] C. Felser, G. H. Fecher, and B. Balke, Angew. Chem. Int. Ed. **46**, 668 (2007).
[3] T. Graf, C. Felser, and S. S. P. Parkin, Prog. Solid State Chem. **39**, 1 (2011).
[4] M. Gillessen and R. Dronskowski, J. Comput. Chem. **30**, 1290 (2009).
[5] M. Gillessen and R. Dronskowski, J. Comput. Chem. **31**, 612 (2010).
[6] I. Žutić, J. Fabian, and S. Das Sarma, Rev. Mod. Phys. **76**, 323 (2004).
[7] M. Bowen, A. Barthélèmy, M. Bibes, E. Jacquet, J. P. Contour, A. Fert, D. Wortmann, and S. Blügel, J. Phys.: Condens. Matter **17**, L407 (2005).
[8] P. J. Webster and K. R. A. Ziebeck, in *Alloys and Compounds of d-Elements with Main Group Elements. Part 2*, edited by H. R. J. Wijn, Landolt-Börnstein, New Series, Group III Vol. 19c, (Springer, Berlin, 1988), pp. 75–184.
[9] K. R. A. Ziebeck and K.-U. Neumann. in *Magnetic Properties of Metals*, edited by H. R. J. Wijn, Landolt-Börnstein, New Series, Group III Vol. 32/c, (Springer, Berlin, 2001), pp. 64–414.
[10] I. Galanakis, P. H. Dederichs, and N. Papanikolaou, Phys. Rev. B **66**, 174429 (2002).
[11] S. Skaftouros, K. Özdoğan, E. Şaşıoğlu, and I. Galanakis, Phys. Rev. B **87**, 024420 (2013).
[12] A. Hirohata and K. Takanashi, J. Phys. D: Appl. Phys. **47**, 193001 (2014).
[13] X. L. Wang, Phys. Rev. Lett. **100**, 156404 (2008).
[14] S. Skaftouros, K. Özdoğan, E. Şaşıoğlu, and I. Galanakis, Appl. Phys. Lett. **102**, 022402 (2013).
[15] A. Jakobsson, P. Mavropoulos, E. Şaşıoğlu, S. Blügel, M. Ležaić, B. Sanyal, and I. Galanakis, Phys. Rev. B **91**, 174439 (2015).

[16] S. Ouardi, G. H. Fecher, C. Felser, and J. Kübler, Phys. Rev. Lett. **110**, 100401 (2013).
[17] J. Y. Rhee and B. N. Harmon, Phys. Rev. B **70**, 094411 (2004).
[18] I. Galanakis, K. Özdoğan, and E. Şaşıoğlu, Phys. Rev. B **86**, 134427 (2012).
[19] G. Y. Gao and K.-L. Yao, Appl. Phys. Lett. **103**, 232409 (2013).
[20] I. M. Tsidilkovski, in *Electron Spectrum of Gapless Semiconductors*, edited by K. von Klitzing, Springer Series in Solid-State Sciences Vol. 116 (Springer, New York, 1996).
[21] M. E. Jamer, B. A. Assaf, G. E. Sterbinsky, D. Arena, L. H. Lewis, A. A. Saúl, G. Radtke, and D. Heiman, Phys. Rev. B **91**, 094409 (2015).
[22] L. R. Testardi, T. Wakiyama, and W. A. Royer, J. Appl. Phys. **48**, 2055 (1977).
[23] S. Ohshima, H. Ishida, T. Wakiyama, and K. Okuyama, Jpn. J. Appl. Phys. **28**, 1362 (1989).
[24] E. Şaşıoğlu, L. M. Sandratskii, and P. Bruno, Phys. Rev. B **70**, 024427 (2004).
[25] K. Koepernik and H. Eschrig, Phys. Rev. B **59**, 1743 (1999).
[26] K. Kopernik, Full Potential Local Orbital Minimum Basis Bandstructure Scheme User's Manual (http://www.fplo.de/download/doc.pdf).
[27] J. P. Perdew, K. Burke, and M. Ernzerhof, Phys. Rev. Lett. **77**, 3865 (1996).
[28] J. P. Perdew and Y. Wang, Phys. Rev. B **45**, 13244 (1992).
[29] H. J. Monkhorst and J. D. Pack, Phys. Rev. B **13**, 5188 (1976).
[30] A. R. Williams, J. Kübler, and C. D. Gelatt, Phys. Rev. B **19**, 6094 (1979).
[31] N. M. Rosengaard and B. Johansson, Phys. Rev. B **55**, 14975 (1997).
[32] S. V. Halilov, H. Eschrig, A. Ya. Perlov, and P. M. Oppeneer, Phys. Rev. B **58**, 293 (1998).
[33] L. M. Sandratskii and P. Bruno, Phys. Rev. B **67**, 214402 (2003).
[34] E. Şaşıoğlu, L. M. Sandratskii, P. Bruno, and I. Galanakis, Phys. Rev. B **72**, 184415 (2005).
[35] S. V. Tyablikov, *Methods of Quantum Theory of Magnetism* (Plenum Press, New York, 1967).
[36] H. B. Callen, Phys. Rev. **130**, 890 (1963).
[37] M. Pajda, J. Kudrnovsky, I. Turek, V. Drchal, and P. Bruno, Phys. Rev. B **64**, 174402 (2001).
[38] G. Bouzerar, J. Kudrnovský, L. Bergqvist, and P. Bruno, Phys. Rev. B **68**, 081203 (2003).
[39] O. K. Andersen, Phys. Rev. B **12**, 3060 (1975).
[40] E. Şaşıoğlu, L. M. Sandratskii, and P. Bruno, Phys. Rev. B **77**, 064417 (2008).
[41] J. Rusz, L. Bergqvist, J. Kudrnovský, and I. Turek, Phys. Rev. B **73**, 214412 (2006).
[42] G. Z. Xu, Y. Du, X. M. Zhang, H. G. Zhang, E. K. Liu, W. H. Wang, and G. H. Wu, Appl. Phys. Lett. **104**, 242408 (2014).
[43] E. Şaşıoğlu, L. M. Sandratskii, and P. Bruno, Phys. Rev. B **71**, 214412 (2005).